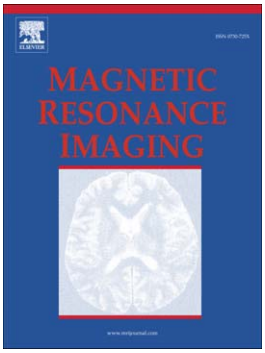

Three-dimensional black-blood T_2 mapping with compressed sensing and data-driven parallel imaging in the carotid artery

Jianmin Yuan, Ammara Usman, Scott A. Reid, Kevin F. King, Andrew J. Patterson, Jonathan H. Gillard, Martin J. Graves

PII: S0730-725X(16)30226-0
DOI: doi:10.1016/j.mri.2016.11.014
Reference: MRI 8669

To appear in: *Magnetic Resonance Imaging*

Received date: 5 November 2016
Revised date: 18 November 2016
Accepted date: 20 November 2016

Please cite this article as: Yuan Jianmin, Usman Ammara, Reid Scott A., King Kevin F., Patterson Andrew J., Gillard Jonathan H., Graves Martin J., Three-dimensional black-blood T_2 mapping with compressed sensing and data-driven parallel imaging in the carotid artery, *Magnetic Resonance Imaging* (2016), doi:10.1016/j.mri.2016.11.014

Three-dimensional black-blood T_2 mapping with compressed sensing and data-driven parallel imaging in the carotid artery

Jianmin Yuan [a*], Ammara Usman [a], Scott A. Reid [b], Kevin F. King [c], Andrew J. Patterson [d], Jonathan H. Gillard [a] and Martin J. Graves [a, d]

[a] Department of Radiology, University of Cambridge, United Kingdom

[b] GE Healthcare, Amersham, United Kingdom

[c] GE Healthcare, Waukesha, Wisconsin, USA

[d] Department of Radiology, Cambridge University Hospitals NHS Foundation Trust, United Kingdom

* Corresponding author:

Jianmin Yuan

Department of Radiology
School of Clinical Medicine
University of Cambridge

Level 5, Box 218, Cambridge University Hospital, Hills Rd.
Cambridge, CB2 0QQ, UK

Tel: +44 (0)1223 767834
Email: jy338@cam.ac.uk

Abstract

Purpose

To develop a 3D black-blood T_2 mapping sequence with a combination of compressed sensing (CS) and parallel imaging (PI) for carotid wall imaging.

Materials and Methods

A 3D black-blood fast-spin-echo (FSE) sequence for T_2 mapping with CS and PI was developed and validated. Phantom experiments were performed to assess T_2 accuracy using a Eurospin Test Object, with different combination of CS and PI acceleration factors. A 2D multi-echo FSE sequence was used as a reference to evaluate the accuracy. The concordance correlation coefficient and Bland-Altman statistics were calculated. Twelve volunteers were scanned twice to determine the repeatability of the sequence and the intraclass correlation coefficient (ICC) was reported. Wall-lumen sharpness was calculated for different CS and PI combinations. Six patients with carotid stenosis >50% were scanned with optimised sequence. The T_2 maps were compared with multi-contrast images.

Results

Phantom scans showed good correlation in T_2 measurement between current and reference sequence ($r = 0.991$). No significant difference was found between different combination of CS and PI accelerations ($p = 0.999$). Volunteer scans showed good repeatability of T_2 measurement (ICC: 0.93, 95% CI 0.84-0.97). The mean T_2 of the healthy wall was 48.0±9.5ms. Overall plaque T_2 values from patients were 54.9±12.2ms. Recent intraplaque haemorrhage and fibrous tissue have higher T_2 values than the mean plaque T_2 values (88.1±6.8ms and 62.7±9.3ms, respectively).

Conclusion

This study demonstrates the feasibility of combining CS and PI for accelerating 3D T_2 mapping in the carotid artery, with accurate T_2 measurements and good repeatability.

Keywords: T_2 mapping, carotid imaging, compressed sensing, parallel imaging

1. Introduction

Globally stroke is one of the most common causes of death and disability[1, 2]. Rupture of the carotid atherosclerotic plaque accounts for around 20% of all ischemic strokes[3]. When looking beyond luminal stenosis, non-invasive MRI shows its ability in assessing plaque vulnerabilities through evaluating high risk components, such as a thin fibrous cap, large lipid rich necrotic core (LRNC), intraplaque haemorrhage (IPH) and neovascularization[4-6].

Multi-contrast MRI has been widely used for characterizing plaque morphology[6, 7]. Plaque components can be differentiated by comparing the signal intensity relative to the adjacent muscle (such as the sternocleidomastoid muscle), in different contrast weighted sequences[8]. For instance, LRNC could be characterized as isointense in time-of-flight (TOF) angiography images, isointense to hyperintense in T_1w and hypointense in T_2w[9-11]; Recent IPH shows hyperintense signal in TOF, T_1w and isointense to hyperintense in T_2w[12]. In addition, quantitative MRI has been introduced in recent years to quantify the relaxation times of plaque components, both in-vivo[9, 13, 14] and ex-vivo[9, 15-17]. Quantitative MRI allows direct measurement of the MR properties of plaque, which mitigates the need to perform relative signal comparisons and overcomes variability introduced by the surface coil position and field non-uniformities[18]. Quantitative measurements may therefore be more suitable across different MRI systems and multi-center studies.

Among these quantitative relaxation values, T_2 and T_2* relaxation times have been reported to be statistically different in plaque components in an ex-vivo study[15]. In-vivo quantitative T_2 mapping has also been used for quantifying the T_2 relaxation time of plaque components, such as fibrous tissue, LRNC, IPH and calcification[13, 19]. Current in-vivo two-dimensional (2D) mapping sequences generally acquire only a few slices with approximately 2mm slice thickness[13, 14]. Three-dimensional (3D) T_2 mapping sequences, in comparison, allow for thinner slices with larger longitudinal coverage[20, 21]. Acquiring 3D *k*-space using dedicated trajectories[22] and receiving the signal from the whole imaging volume enables improved scan efficiency and achieves higher SNR compared to 2D methods.

This study applies improved motion-sensitized driven-equilibrium (iMSDE) as a preparation pulse to suppress blood flow, furthermore, the intra-pulse durations within the iMSDE preparation are varied to change the effective echo time (TE) and enable subsequent T_2 quantification. Unlike 2D T_2 mapping sequences, which acquire multiple TEs in one repetition time (TR), 3D T_2 mapping sequences normally repeat the same sequence multiple times with different effective TEs, resulting in long overall scan times. Parallel imaging can reduce the acquisition time, and is a reproducible and robust method[23, 24], however, the achievable acceleration is limited by the number of coils and the noise amplification.

Compressed sensing (CS) is an additional method of scan acceleration[25-27], which is based upon the compressibility of the MR data. This method has previously been used in carotid morphological imaging[27]. In addition, patient movement during long scanning times cannot be eliminated especially when the images at different echo time are acquired sequentially. This requires additional image coregistration which may reduce the accuracy of T_2 measurement. The sequence in this study used an interleaved acquisition so that the images at different echo times are intrinsically coregistered.

This study evaluates an iMSDE prepared, black blood, 3D T_2 mapping sequence with the combination of compressed sensing and data-driven parallel imaging[28]. Phantom studies and healthy volunteer scans were carried out to evaluate the accuracy and repeatability of this sequence. Patients with carotid stenosis >50% were also scanned using this sequence and the T_2 maps were compared with conventional multi-contrast images.

2. Materials and Methods

2.1 Sequence

An iMSDE preparation scheme, with variable TE, was combined with a 3D fast spin echo (FSE) readout to achieve black-blood T_2 mapping, as shown in figure 1. A variable flip angle refocusing train was used in the readout[22]. The iMSDE preparation is comprised of two non-selective 90° pulses with two composite 180° pulses between them, together with motion sensitive gradients along the X, Y and Z axes between the pulses[29]. The first-order moment was empirically set to 412 $mTms^2/m$. Fat saturation was achieved by using an Adiabatic SPectral Inversion Recovery (ASPIR) pulse before the FSE readout. A radial view ordering scheme was used to achieve the shortest possible readout TE[22]. The total TE for the sequence is the sum of the iMSDE preparation TE_{iMSDE} and the FSE readout TE_{FSE}. By changing the time interval within the iMSDE preparation ($TE_{iMSDE} = 4\tau$), images with different TEs were achieved. Three different values of TE_{iMSDE} were interleaved in a single acquisition. The effect of the noise baseline was corrected by computing the power images ($I_c{}^2$) using Miller's algorithm[30]:

$$I_c(TE)^2 = I(TE)^2 - I_n(TE)^2 \quad (1)$$

where $I(TE)$ and $I_n(TE)$ are the signal and background noise intensity at each echo. The T_2 map was then generated on a voxelwise basis by fitting the following equation to the three TE images using the Levenberg-Marquardt algorithm nonlinear least-squares algorithm:

$$I_c(TE)^2 = I_0{}^2 e^{-2TE/T_2} \quad (2)$$

where $I_c(TE)^2$ is the corrected power voxel signal at different TE, and $I_0{}^2$ is the estimated power signal at TE=0.

The FSE readout was further modified to allow a combined parallel imaging and compressed sensing acquisition. A self-calibrated data-driven parallel imaging reconstruction method, Autocalibrated Reconstruction of Cartesian (ARC) data[31], was used. This method uses a full 3D kernel to synthesize the non-acquired data in the *k*-space from neighbouring acquired data in three dimensions[31] and as well as utilising CS reconstruction[28, 32]. An example of a 3D *k*-space acquired by ARC is shown in Figure 2(a) and (b). Figure 2(a) shows the *k*-space sampling pattern for a 224×40 ($k_y \times k_z$) matrix size with an ARC acceleration factor of 2 (2×1 in $k_y \times k_z$ direction). Figure 2(b) shows the acceleration factor of 4 (2×2). In ARC, the outer region of *k*-space is uniformly undersampled whilst the auto-calibration center is fully sampled[28]. The auto-calibration center was set to 32×32 in this study. For compressed sensing, the non-calibrated ARC *k*-space was further undersampled using a Gaussian pseudo-random distribution. Figure 2(c) and (d) shows the *k*-space using a CS factor 1.5 together with ARC accelerations of 2×1 and 2×2 respectively. Figure 2(e) and (f) show a higher CS factor of 2.0. In the reconstruction, a non-linear conjugate gradient solver with fifteen iteration loops was applied to minimise the L1-norm of the following object function for each channel and each echo[25]:

$$\hat{m} = minimize\{\|Fm - y\|_2^2 + \lambda\|\Psi m\|_1\} \quad (3)$$

where $\| \quad \|_1$ means the L1-norm, Ψ is the sparsifying transform implemented as a nearest neighbor finite difference of the complex image m, F is the Fourier transform operator and y is the acquired *k*-space data. The consistency of acquired data was maintained by substituting the acquired *k*-space data back into the new *k*-space after each iteration. In this study, ARC and CS were combined in a serial approach with CS as the first step and ARC as the second step[28]. This enabled separate reconstruction of each method which is more compatible with the current existing ARC implementation, allowing for an easy combination of different CS and ARC acceleration factors. More details of the acquisition and reconstruction can be found in [28, 32].

2.2 MRI Experiments

All the imaging experiments were performed using a 3T system (MR750, GE Healthcare, Waukesha, WI), using a four channel phased-array neck coil (PACC, MachNet, Roden, The Netherlands).

2.3 Phantom study

The sequence was initially tested using the Eurospin Test Object (TO5) phantom (Diagnostic Sonar, Livingston, UK) which contains calibrated gels with known relaxivity values at 19º C. Nine gels were selected with a range of T_2 values which represent the T_2 values of plaque components previously reported in the literature (ranging from 52ms to 143ms). A three echo FSE sequence (TR = 2000ms, TE = 21.6, 51.6, 81.6ms) with the combination of two ARC values (2×1 and 2×2), without CS and with CS factors of 1.5 and 2.0 were used to acquire a total of six T_2 maps. The imaging matrix was 224×224×40, with field-of-view of 140×140×56mm^3. A 2D multi-echo fast spin echo (MEFSE) sequence was acquired for comparison, with TR = 2000ms and eight TEs from 8.6ms to 68.8ms with 8.6ms intervals. The imaging matrix for 2D MEFSE was 224×224, the field-of-view was 140×140mm^2 and the slice thickness was 2mm.

2.4 Volunteer study

Twelve healthy volunteers (eight men, mean age 34, range: 24-55 years) were recruited in this study, these volunteer experiments were conducted under an existing research ethics agreement and all volunteers gave informed written consent. The volunteers were scanned with ARC 2×1 and without CS once, and with a CS factor of 1.5 twice. The repeated scan was used to determine the repeatability of the T_2 measurements, the average interval between the two scans was 14 days (range 7 to 28 days). Other scanning parameters of this sequence are listed in the last column of Table 1.

2.5 Patient study

Six patients (four men, mean age 80, range: 74-87 years) who had a carotid stenosis of at least 50% on Duplex ultrasound underwent this examination. A vacuum pillow was placed around the head and neck to minimise the movement. The standard protocol included multi-contrast 3D sequences in the coronal plane: a 3D time-of-flight (TOF) sequence, pre- and post-contrast DANTE prepared[33] 3D FSE sequence and pre-contrast MR-Direct Thrombus Imaging sequence (MR-DTI)[34]. The center of the imaging volume was positioned over the carotid bifurcation. Details of the scanning parameters are summarized in Table 1. The T_2 mapping sequence with a combination of CS factor of 1.5 and ARC 2×1 was used for the patient scanning. This separate study protocol was reviewed and approved by a local ethics committee and written informed consent was obtained from each patient.

2.6 Image analysis

The acquired images were first interpolated to 512×512×80, and then reformatted into the axial plane with a pixel size of 0.2×0.2×0.3mm^3. For the phantom scans, regions of interest were defined within each gel and the mean and standard deviation (sd) of the T_2 values were recorded for each ARC and CS

combination. For the volunteer scans, the analysis was performed on 10 contiguous slices of the common carotid artery (CCA) below the bifurcation on both sides. Vessel wall and lumen were manually segmented using a DICOM viewer (OsiriX 5.5.2, Pixmeo, Geneva, Switzerland). The ARC 2×1 without CS accelerated *k*-space data of the volunteers was saved and used off-line for simulating higher ARC and CS acceleration factors. Simulation experiments were performed using in-house software developed in MATLAB R2015b (MathWorks, Natick, Massachusetts, USA). To quantify the blurring due to the ARC and CS acceleration, wall-lumen sharpness from the first echo was calculated for each combination[35]. A single axial slice of the CCA 5mm below the bifurcation was chosen for the sharpness calculation. The image was first bilinearly interpolated at a factor of six to increase the image matrix, resulting in an interpolated pixel size of $0.03\times0.03mm^2$. An intensity profile perpendicular to the vessel wall was drawn from the wall to the lumen. To determine image sharpness a synthetic image was created with the relative signal intensity of the lumen set to zero and the highest signal intensity in the vessel wall set to one. The wall-lumen sharpness was calculated by

$$\text{Sharpness} = 1/d \ (mm^{-1}) \tag{4}$$

Where *d* is the distance between pixels at an intensity between 0.8 and 0.2.

2.7 Data analysis

The statistical analysis was performed using R (version 3.2.2)[36]. The Shapiro–Wilk's test was used to test normality assumptions. Normally distributed data was presented as mean±sd. A one-way ANOVA was used to compare T_2 measurements with different ARC and CS combinations. The concordance correlation coefficient (CCC) and Bland-Altman plots were used to evaluate the correlation between 2D and 3D methods[37]. For the volunteer scans, the coefficient of variation (CoV: the ratio of the SD divided by the mean value) of T_2 values within each of the vessel wall with different CS and ARC combination were calculated. The intraclass correlation coefficient (ICC) was used to evaluate the agreement between two repeated scans. Statistical significance was defined as a p-value < 0.05.

3 Results

3.1 Phantom study

Figure 3(a) shows the measured T_2 values with different combinations of ARC and CS factors, the quantitative comparison found no significant difference between the different combinations ($p = 0.999$). Figure 3(b) shows the phantom T_2 values measured by 3D iMSDE FSE with ARC 2×1 and CS factor of

1.5 compared to the standard 2D MESE. A high correlation was noted between the two sequences for T_2 values ranging from 52ms to 143ms (r = 0.991). The CCCs between 2D and other 3D ARC and CS combinations were all above 0.9. Figure 3(c) shows the Bland-Altman plot comparing the two scans, with the bias of 3.0ms and 95% limits of agreement -3.1 and 9.0ms.

3.2 Volunteer study

All twelve volunteers (100%) completed the scans with good blood suppression achieved in all images. Figure 4(a) shows a volunteer image without compressed sensing (ARC 2×1), (b-f) shows the reconstruction image from retrospectively subsampled *k*-space from (a). The vessel wall boundaries become blurred with increasing CS factors, and the noise level increases with increasing ARC parallel acceleration factors. The wall-lumen sharpness of each combination from 24 arteries in the 12 volunteers is shown in Figure 5. There was no difference between the actual scan and simulated data in ARC 2×1 and CS 1.5 combination ($1.7mm^{-1}$ vs. $1.7mm^{-1}$). Figure 5(a) shows how the image sharpness was defined. In figure 5(b), the non-CS accelerated image has the highest wall-lumen sharpness ($1.9mm^{-1}$). With ARC 2×1 and CS 1.5, the image has a higher wall-lumen sharpness compared with CS 2.0 ($1.7mm^{-1}$ vs. $1.4mm^{-1}$).

Figure 6(a) shows the T_2 map from one volunteer with CS 1.5 and ARC 2×1. Figure 6(b) shows the CoV of T_2 values of measured slices in each combination. CoV remains similar when CS factor is below 1.5 and increases when CS factor increased to 2.0. ARC 2×2 has a higher CoV compared to ARC 2×1. The mean T_2 value for the volunteer carotid wall was 48.0±9.5ms. Good repeatability was found between the two scans (ICC: 0.93, 95% CI 0.84-0.97). According to the noise level from figure 4 and wall-lumen sharpness evaluation in figure 5, a combination of ARC 2×1 and CS factor of 1.5 was chosen for the patient study.

3.3 Patient study

Five of the six patients (83%) completed the scans. Eight carotid plaques were found in the five patients. Recent IPH was found in four plaques, and fibrous tissue was found in two of the plaques. The overall T_2 values of the plaques were 54.9±12.2ms. The mean wall-lumen sharpness of the 10 CCAs from these five patients was $1.5±0.3mm^{-1}$, which is similar to volunteer scans.

Figure 7 shows an example of a right carotid plaque from a patient. The white arrow shows the region of hyperintensity in T_1w, hypointensity in post-contrast T_1w, and hyperintensity signal in MR-DTI. This region was indicative of recent IPH. T_2 mapping shows higher T_2 values in the recent IPH (88.1±6.8ms) compared to other plaque regions. Figure 8 shows a plaque with fibrous tissue inside. The fibrous shows

hyperintense signal in post-contrast T_1w and the third echo of T_2mapping sequence (T_2w). The T_2 values for the fibrous tissue were 62.7±9.3ms.

4. Discussion

This study, for the first time, shows the combination of compressed sensing and parallel imaging to reduce the time of 3D T_2 mapping to a clinically acceptable acquisition time (7min 48s). T_2 mapping sequences in carotid plaque have shown the ability to differentiate plaque components[15], which could be used for plaque segmentation and identification of high risk components[13, 19]. Whilst compressed sensing[26, 27, 38, 39] and parallel imaging[23, 24, 26, 40] have been introduced for multi-contrast carotid vessel wall imaging, these acceleration techniques have not yet been reported for 3D T_2 mapping. In this study, the measured T_2 values from volunteers' healthy carotid vessel walls and plaque components from patients are similar to previous studies[13, 14]. Furthermore, this T_2 mapping sequence could also be used to simultaneously obtain PD and T_2 weighted images, with the first echo of TE/TR = 21.6/2000ms, and the third echo of TE/TR = 81.6/2000ms.

Rapid 2D T_2 mapping can be achieved by using multi-echo fast spin echo sequences [13-15], which can acquire images with different TEs in one TR. However, it becomes challenging when extending into 3D, since most 3D sequences do not allow interleaved multi-echo acquisitions and the *k*-space view-ordering is more complicated. To achieve T_2 mapping, one method is to change the TE in the preparation pulse, either in a T_2 preparation[21] or preferably combined in a black-blood iMSDE preparation[20]. Studies have demonstrated that both FSE[21] and GRE[20] based readouts could achieve good T_2 mapping results. The long TR in FSE based T_2 mapping sequences allows the magnetisation to fully recover after each readout segment, which enables images with different TEs to be acquired in an interleaved fashion. Therefore the "echoes" are intrinsically registered. In comparison to acquiring images with different TEs sequentially, this method does not need additional image registration in the post- processing which could induce extra variability[20].

The main limitation of this study is the absence of histological validation of the plaques. Since the participating patients were asymptomatic, they were not scheduled for surgery. However, the phantom validation in this study showed good accuracy and the measurements of carotid wall T_2 values in both volunteers and patients are in good agreement with other studies[13-15]. The second limitation is that the study only has a small number of patients. A third limitation is that cardiac gating was not used in these sequences. However, Zhu. et al showed that ungated sequences could achieve comparable vessel signal and contrast-to-noise ratio (SNR/CNR) than gated sequence in black blood FSE based carotid imaging[41]. The accuracy of gated and ungated T_2 mapping sequences needs further exploration. The

fourth limitation is that the CS reconstruction algorithm used in this study was developed for general application, and not specifically optimised for imaging the carotid wall. Further optimisation of the reconstruction parameters could potentially improve image quality, however this is outside the scope of this study. The last limitation would be that in this study, a specific CS reconstruction and sequential combination of CS and ARC were used, which may not be the optimum process. There are also other CS algorithms[42-44] and different combination of CS with PI[45, 46] or other acceleration methods[47, 48] existing in the literature that might worth exploring. However this is outside of the scope of current work. A recent paper described a combination of CS and principal component analysis could derive T_2 information from a single scan[49]. However the feasibility of this method in carotid plaque imaging needs to be explored as blood suppression is necessary for vessel wall imaging. The methods used in the current study is an straightforward implementation of a black-blood sequence with a combined PI+CS reconstruction method.

5. Conclusion

This study demonstrates the combination of CS and ARC for accelerating 3D blood-suppressed T_2 mapping in the carotid artery, using an interleaved variable TE iMSDE based black-blood preparation scheme. These acceleration techniques reduce the 3D T_2 mapping sequence to a clinically acceptable acquisition time of 7min 48s for three echoes with a high acquired spatial resolution of $0.6\times0.6\times1.4mm^3$.

6. Conflicts of interest

Scott Reid and Kevin King are employees of GE Healthcare.

7. Acknowledgements

The project was supported by the Addenbrooke's Charitable Trust and the NIHR comprehensive Biomedical Research Centre award to Cambridge University Hospitals NHS Foundation Trust in partnership with the University of Cambridge.

8. References

[1] Truelsen T, Piechowski‐Jóźwiak B, Bonita R, Mathers C, Bogousslavsky J, Boysen G. Stroke incidence and prevalence in Europe: a review of available data. European journal of neurology 2006;13:581-98.
[2] Hoyert D L, Xu J. Deaths: preliminary data for 2011. Natl Vital Stat Rep 2012;61:1-51.
[3] Wityk R, Lehman D, Klag M, Coresh J, Ahn H, Litt B. Race and sex differences in the distribution of cerebral atherosclerosis. Stroke 1996;27:1974-80.

[4] Saam T, Ferguson M, Yarnykh V, Takaya N, Xu D, Polissar N, et al. Quantitative evaluation of carotid plaque composition by in vivo MRI. Arteriosclerosis, thrombosis, and vascular biology 2005;25:234-9.
[5] Yuan C, Mitsumori L M, Ferguson M S, Polissar N L, Echelard D, Ortiz G, et al. In vivo accuracy of multispectral magnetic resonance imaging for identifying lipid-rich necrotic cores and intraplaque hemorrhage in advanced human carotid plaques. Circulation 2001;104:2051-6.
[6] Kerwin W S. Carotid artery disease and stroke: assessing risk with vessel wall MRI. ISRN cardiology 2012;2012:
[7] Cai J-M, Hatsukami T S, Ferguson M S, Small R, Polissar N L, Yuan C. Classification of human carotid atherosclerotic lesions with in vivo multicontrast magnetic resonance imaging. Circulation 2002;106:1368-73.
[8] Usman A, Sadat U, Graves M J, Gillard J H. Magnetic resonance imaging of atherothrombotic plaques. Journal of Clinical Neuroscience 2015;22:1722-6.
[9] LaMuraglia G M, Southern J F, Fuster V, Kantor H L. Magnetic resonance images lipid, fibrous, calcified, hemorrhagic, and thrombotic components of human atherosclerosis in vivo. Circulation 1996;94:932-8.
[10] Underhill H R, Yarnykh V L, Hatsukami T S, Wang J, Balu N, Hayes C E, et al. Carotid Plaque Morphology and Composition: Initial Comparison between 1.5-and 3.0-T Magnetic Field Strengths 1. Radiology 2008;248:550-60.
[11] Sadat U, Teng Z, Young V, Walsh S, Li Z, Graves M, et al. Association between biomechanical structural stresses of atherosclerotic carotid plaques and subsequent ischaemic cerebrovascular events–a longitudinal in vivo magnetic resonance imaging-based finite element study. European Journal of Vascular and Endovascular Surgery 2010;40:485-91.
[12] Fabiano S, Mancino S, Stefanini M, Chiocchi M, Mauriello A, Spagnoli L G, et al. High-resolution multicontrast-weighted MR imaging from human carotid endarterectomy specimens to assess carotid plaque components. European radiology 2008;18:2912-21.
[13] Biasiolli L, Lindsay A C, Chai J T, Choudhury R P, Robson M D. In-vivo quantitative T2 mapping of carotid arteries in atherosclerotic patients: segmentation and T2 measurement of plaque components. Journal of Cardiovascular Magnetic Resonance 2013;15:1-9.
[14] Proniewski B, Miszalski-Jamka T, Jazwiec P. In vivo T2-mapping and segmentation of carotid artery plaque components using magnetic resonance imaging at 1.5 T. Computing in Cardiology Conference (CinC), 2014. 2014. 921-4
[15] Degnan A J, Young V E, Tang T Y, Gill A B, Graves M J, Gillard J H, et al. Ex vivo study of carotid endarterectomy specimens: quantitative relaxation times within atherosclerotic plaque tissues. Magnetic resonance imaging 2012;30:1017-21.
[16] Dalager-Pedersen S, Falk E, Ringgaard S, Kristensen I B, Pedersen E M. Effects of temperature and histopathologic preparation on the size and morphology of atherosclerotic carotid arteries as imaged by MRI. Journal of magnetic resonance imaging 1999;10:876-85.
[17] Morrisett J, Vick W, Sharma R, Lawrie G, Reardon M, Ezell E, et al. Discrimination of components in atherosclerotic plaques from human carotid endarterectomy specimens by magnetic resonance imaging ex vivo. Magnetic resonance imaging 2003;21:465-74.
[18] Biasiolli L, Lindsay A C, Choudhury R P, Robson M D. Loss of fine structure and edge sharpness in fast‐spin‐echo carotid wall imaging: measurements and comparison with multiple‐spin‐echo in normal and atherosclerotic subjects. Journal of Magnetic Resonance Imaging 2011;33:1136-43.
[19] Chai J T, Biasiolli L, Li L, Alkhalil M, Galassi F, Darby C, et al. Lipid-rich Core Quantification in Carotid Atherosclerosis Using MRI T2 Mapping-Relation to Clinical Presentation and Plaque Macrophage Activation. Circulation 2015;132:A11833-A.
[20] Coolen B F, Poot D H, Liem M I, Smits L P, Gao S, Kotek G, et al. Three‐dimensional quantitative T1 and T2 mapping of the carotid artery: Sequence design and in vivo feasibility. Magnetic resonance in medicine 2015;

[21] Smit H, Leeuw H d, Guridi R P, Poot D H J, Vogel M, Lugt A v d, et al. T2 mapping in the carotid artery with T2 prepared signal stabilized 3D fast spin echo. Presentation at ESMRMB 2013 2013;
[22] Busse R F, Brau A, Vu A, Michelich C R, Bayram E, Kijowski R, et al. Effects of refocusing flip angle modulation and view ordering in 3D fast spin echo. Magnetic resonance in medicine 2008;60:640-9.
[23] Saam T, Raya J G, Cyran C C, Bochmann K, Meimarakis G, Dietrich O, et al. High resolution carotid black-blood 3T MR with parallel imaging and dedicated 4-channel surface coils. Journal of Cardiovascular Magnetic Resonance 2009;11:1.
[24] Grimm J M, Schindler A, Freilinger T, Cyran C C, Bamberg F, Yuan C, et al. Comparison of symptomatic and asymptomatic atherosclerotic carotid plaques using parallel imaging and 3 T black-blood in vivo CMR. J Cardiovasc Magn Reson 2013;15:44.
[25] Lustig M, Donoho D, Pauly J M. Sparse MRI: The application of compressed sensing for rapid MR imaging. Magnetic resonance in medicine 2007;58:1182-95.
[26] Otazo R, Feng L, Lim R, Duan Q, Wiggins G, Sodickson D K, et al. Accelerated 3D carotid MRI using compressed sensing and parallel imaging. Journal of Cardiovascular Magnetic Resonance 2010;12:1.
[27] Li B, Dong L, Chen B, Ji S, Cai W, Wang Y, et al. Turbo fast three‐dimensional carotid artery black‐blood MRI by combining three‐dimensional MERGE sequence with compressed sensing. Magnetic Resonance in Medicine 2013;70:1347-52.
[28] King K, Xu D, Brau A, Lai P, Beatty P, Marinelli L. A new combination of compressed sensing and data driven parallel imaging. Proceedings of 18th Annual Meeting of ISMRM, Stockholm, Sweden. 2010. 4881
[29] Wang J, Yarnykh V L, Hatsukami T, Chu B, Balu N, Yuan C. Improved suppression of plaque‐mimicking artifacts in black‐blood carotid atherosclerosis imaging using a multislice motion‐sensitized driven‐equilibrium (MSDE) turbo spin‐echo (TSE) sequence. Magnetic resonance in medicine 2007;58:973-81.
[30] Miller A J, Joseph P M. The use of power images to perform quantitative analysis on low SNR MR images. Magnetic resonance imaging 1993;11:1051-6.
[31] Beatty P, Brau A, Chang S, Joshi S, Michelich C, Bayram E, et al. A method for autocalibrating 2-D accelerated volumetric parallel imaging with clinically practical reconstruction times. Proc Intl Soc Magn Res Med. 2007. 1749
[32] Pandit P, Rivoire J, King K, Li X. Accelerated T1ρ acquisition for knee cartilage quantification using compressed sensing and data-driven parallel imaging: A feasibility study. Magnetic resonance in medicine 2016;75:1256-61.
[33] Li L, Miller K L, Jezzard P. DANTE‐prepared pulse trains: A novel approach to motion‐sensitized and motion‐suppressed quantitative magnetic resonance imaging. Magnetic resonance in medicine 2012;68:1423-38.
[34] Priest A N, Joubert I, Hilborne S, Hunter S, Bowden D J, Graves M J, et al. MR Direct Thrombus Imaging with optimised signal and improved lipid suppression. Proceedings of 21st Annual Meeting of ISMRM, Salt Lake City, Utah, USA. 2013. 1280
[35] Larson A C, Kellman P, Arai A, Hirsch G A, McVeigh E, Li D, et al. Preliminary investigation of respiratory self‐gating for free‐breathing segmented cine MRI. Magnetic resonance in medicine 2005;53:159-68.
[36] Team R C, ISBN 3-900051-07-0, 2014.
[37] Bland J M, Altman D. Statistical methods for assessing agreement between two methods of clinical measurement. The lancet 1986;327:307-10.
[38] Tao Y, Rilling G, Davies M, Marshall I. Carotid blood flow measurement accelerated by compressed sensing: Validation in healthy volunteers. Magnetic resonance imaging 2013;31:1485-91.
[39] Makhijani M K, Balu N, Yamada K, Yuan C, Nayak K S. Accelerated 3D MERGE carotid imaging using compressed sensing with a hidden Markov tree model. Journal of Magnetic Resonance Imaging 2012;36:1194-202.

[40] Sumi T, Sumi M, Van Cauteren M, Kimura Y, Nakamura T. Parallel imaging technique for the external carotid artery and its branches: Comparison of balanced turbo field echo, phase contrast, and time‐of‐flight sequences. Journal of Magnetic Resonance Imaging 2007;25:1028-34.
[41] Zhu C, Graves M J, Sadat U, Young V E, Gillard J H, Patterson A J. Comparison of Gated and Ungated Black-Blood Fast Spin-echo MRI of Carotid Vessel Wall at 3T. Magnetic Resonance in Medical Sciences 2015;15(3):266-72.
[42] Chartrand R. Fast algorithms for nonconvex compressive sensing: MRI reconstruction from very few data. 2009 IEEE International Symposium on Biomedical Imaging: From Nano to Macro. 2009. 262-5
[43] Badnjar J. Comparison of Algorithms for Compressed Sensing of Magnetic Resonance Images. arXiv preprint arXiv:1502.02182 2015;
[44] Ma S, Yin W, Zhang Y, Chakraborty A. An efficient algorithm for compressed MR imaging using total variation and wavelets. Computer Vision and Pattern Recognition, 2008. CVPR 2008. IEEE Conference on. 2008. 1-8
[45] Lustig M, Alley M, Vasanawala S, Donoho D, Pauly J. L1 SPIR-iT: autocalibrating parallel imaging compressed sensing. Proc Intl Soc Mag Reson Med. 2009. 379
[46] Otazo R, Kim D, Axel L, Sodickson D K. Combination of compressed sensing and parallel imaging for highly accelerated first‐pass cardiac perfusion MRI. Magnetic Resonance in Medicine 2010;64:767-76.
[47] Hollingsworth K G. Reducing acquisition time in clinical MRI by data undersampling and compressed sensing reconstruction. Physics in medicine and biology 2015;60:R297.
[48] Kuestner T, Wurslin C, Gatidis S, Martirosian P, Nikolaou K, Schwenzer N, et al. MR image reconstruction using a combination of Compressed Sensing and partial Fourier acquisition: ESPReSSo. IEEE transactions on medical imaging 2016;35(11):2447-58.
[49] Tamir J I, Uecker M, Chen W, Lai P, Alley M T, Vasanawala S S, et al. T2 shuffling: Sharp, multicontrast, volumetric fast spin‐echo imaging. Magnetic resonance in medicine 2016;

Table 1. Imaging protocol for 3D multi-contrast MRI.

Sequence	TOF	Pre/Post-contrast DANTE T_1w FSE	MR-DTI	iMSDE T_2 mapping
Flip angle (°)	20	Variable flip angle	30	Variable flip angle
Echo train length	-	24	-	40
TE/TR (ms)	2.2/5.9	16.9/540	4.2/8.6	21.6, 51.6 and 81.6/2000
Acquired Matrix size	256×256×32	224×224×48	160×160×66	224×224×40
Acquired pixel size (mm^3)	0.5×0.5×2	0.6×0.6×1.4	0.5×0.5×1.4	0.6×0.6×1.4
Acquisition Time	1min 35s	2×6min 26s	4min 42s	7min 48s

TOF: time-of-flight; DANTE: Delay alternating with nutation for tailored excitation; iMSDE: Improved motion-sensitized driven-equilibrium; FSE: fast spin echo; MR-DTI: MR-direct thrombus imaging.

Figure legends

Figure 1. 3D iMSDE prepared compressed sensing FSE. The overall echo times (TE_1, TE_2, …, TE_n) are achieved by varying the echo time ($TE_{iMSDE} = 4\tau$) in the iMSDE preparation.

Figure 2. Undersampled *k*-space patterns with different combinations of ARC ($k_y \times k_z$) and CS factors.

Figure 3. (a) Measured T_2 values of Eurospin phantom using different combination of ARC and CS acceleration factors. (b) Concordance correlation of T_2 measurements obtained using 3D iMSDE FSE (ARC2×1 and CS1.5) and 2D MEFSE. (c) Bland-Altman plot of the difference versus the mean of the T_2 values using 3D iMSDE FSE (ARC2×1 and CS1.5) and 2D MEFSE.

Figure 4. Simulation experiment comparing ARC and increasing CS accelerations in a healthy volunteer. The scaled top-right corner images are the reformatted axial projections.

Figure 5. (a) With blood suppression the signal intensity drops from wall to lumen. The line profile was drawn from wall to lumen to determine the wall-lumen sharpness. (b) Compares wall-lumen sharpness for the volunteer cohort using ARC and CS combinations measured in both carotid arteries (n=24 arteries).

Figure 6. (a): Images of a volunteer with different echo times and the resultant T_2 map (with ARC2×1 and CS1.5). (b): Plots the Coefficient of Variation (CoV, within each of the vessel wall) and compares the ARC and CS combinations from both volunteers arteries (n=24).

Figure 7. An example of recent IPH (while arrow) identified using a multi-contrast MRI protocol. Recent IPH shows higher T_2 values than the surrounding plaque region. (Gd = Gadobutrol Contrast Agent, DTI = Direct Thrombus Imaging, IPH = Intraplaque Haemorrhage)

Figure 8. Multi-contrast MRI shows fibrous tissue in the plaque. The fibrous tissue has higher T_2 values than the surrounding plaque components. (Gd = Gadobutrol Contrast Agent, TOF = Time of Flight)

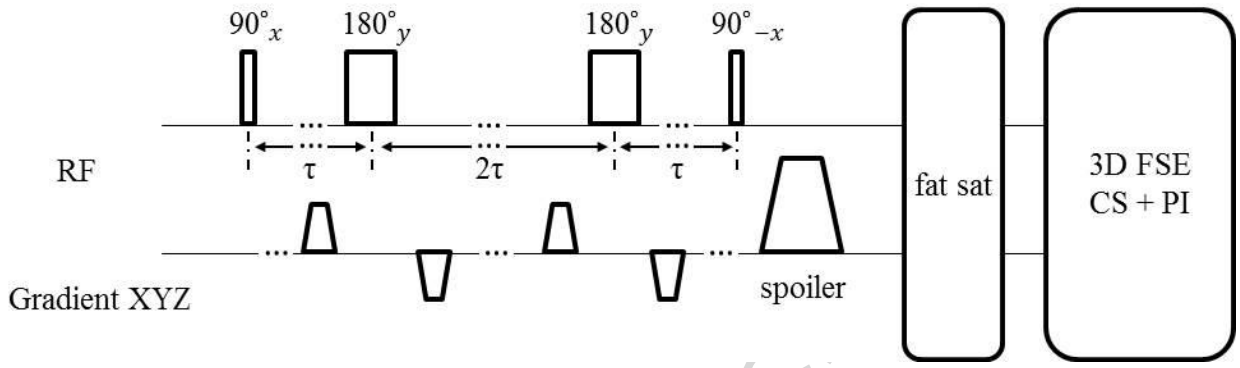

Figure 1

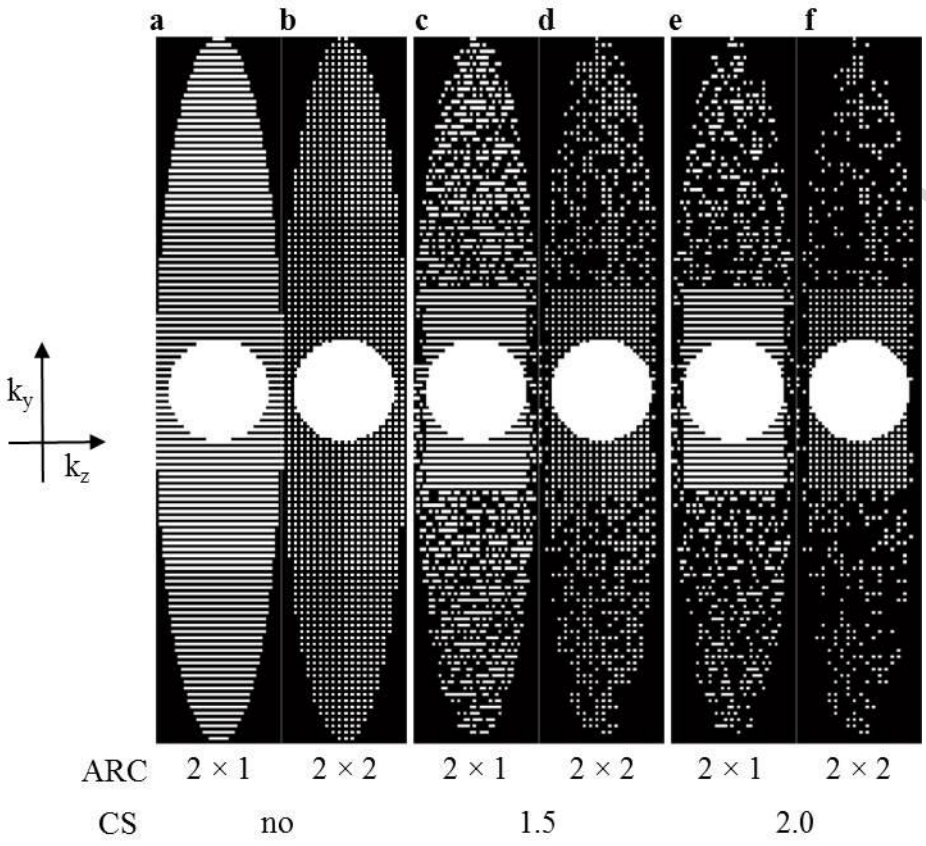

Figure 2

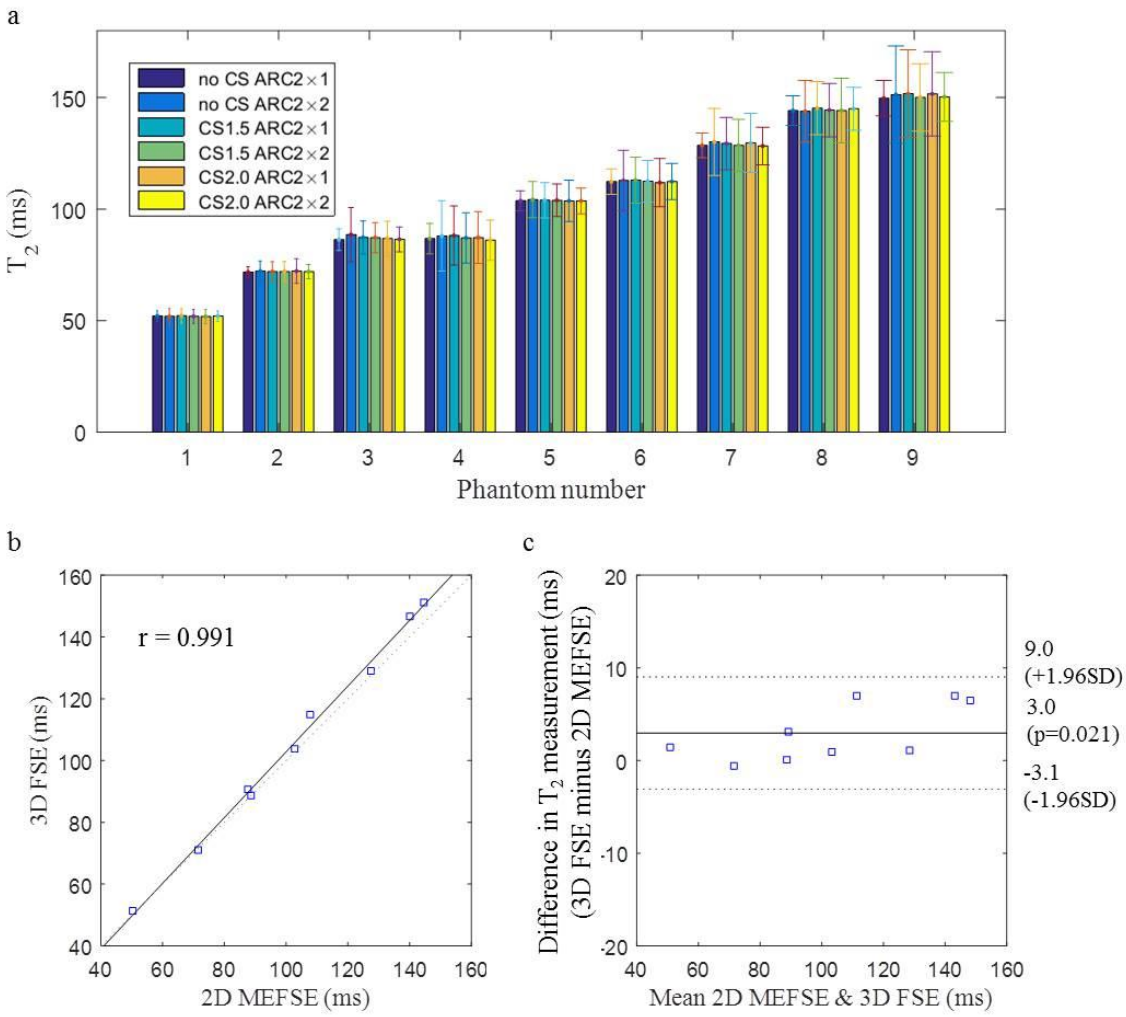

Figure 3

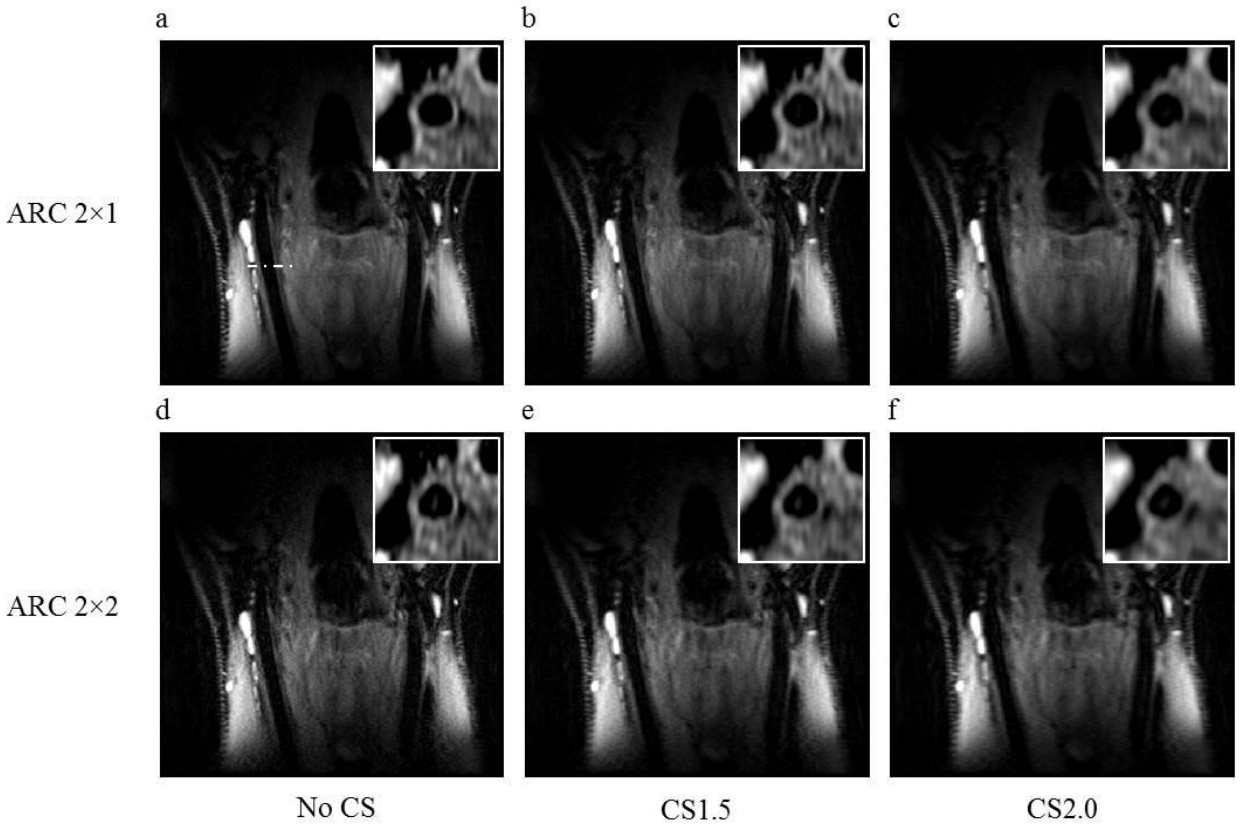

Figure 4

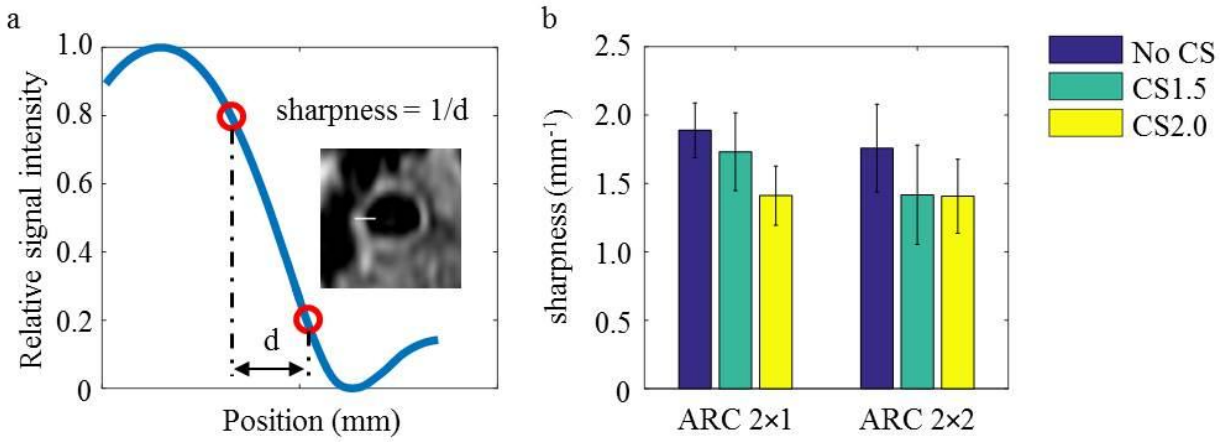

Figure 5

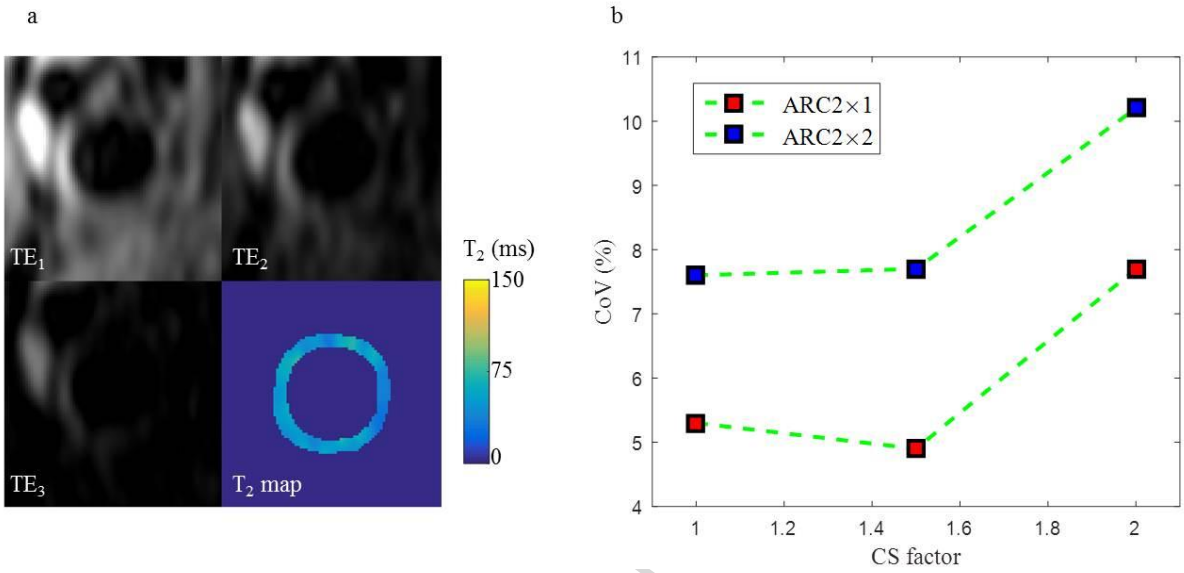

Figure 6

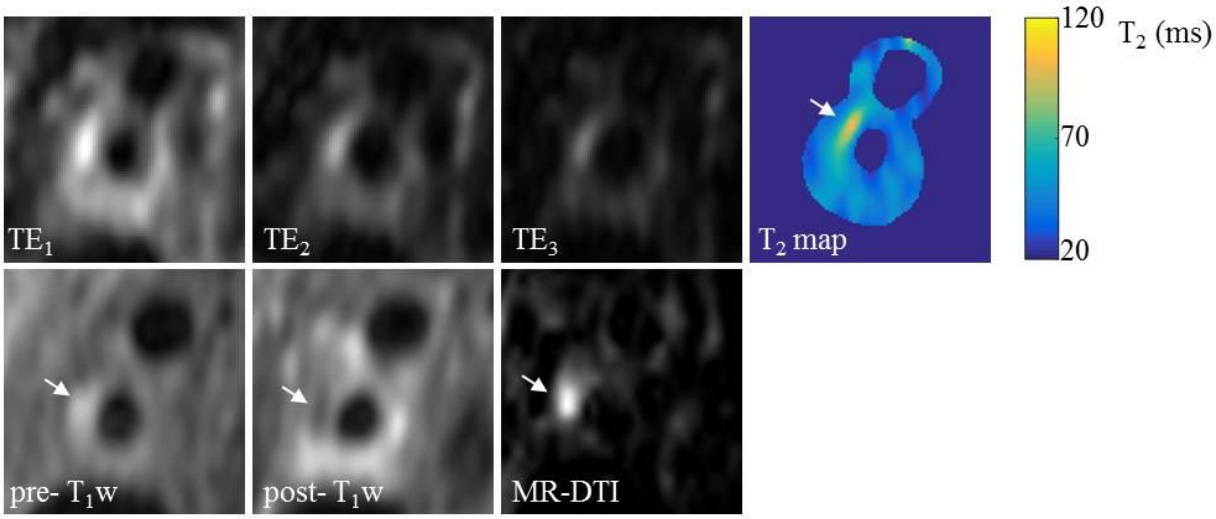

Figure 7

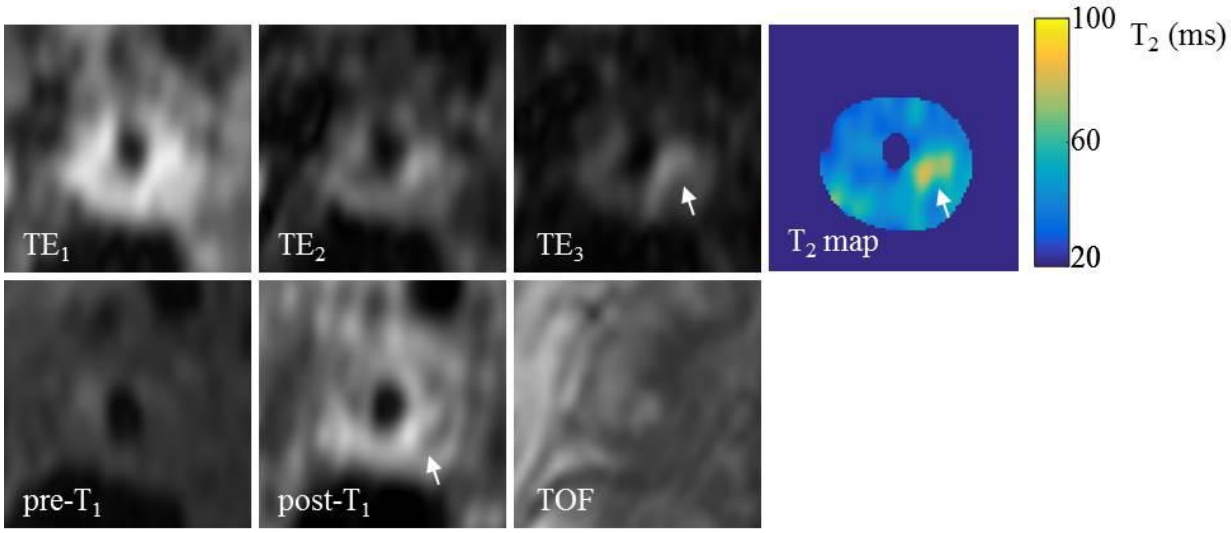

Figure 8